Velocity Field of a Cylinder in the Wake of a Rotor in Forward Flight

S. G. Liou,* N. M. Komerath,† and H. M. McMahon‡
Georgia Institute of Technology, Atlanta, Georgia 30332

The rotor and the airframe of a rotorcraft can have severe effects on each other because of flowfield interactions. Data on flowfield characteristics have been obtained using laser velocimetry in an attempt to identify and interpret the features of such interactions. This paper summarizes previous results on the flowfield of the rotor and then describes the effects of the rotor wake on the flowfield around an airframe model. A circular cylinder with a hemispherical nose is used as the airframe model and is instrumented with static pressure taps and flush-mounted microphones. A two-bladed teetering rotor is suspended above it in a wind tunnel. The periodic and time-averaged velocity fields are measured along lines parallel to the airframe axis at a rotor advance ratio of 0.1 and a rotor tip Mach number of 0.29. The dominant features in the velocity distribution over the airframe are seen to be linked to vortex interactions with the airframe surface. The tip vortex and the trailing vortex sheet are seen to be displaced in opposite directions by the airframe. Secondary vortex generation phenomena are observed near the airframe surface during vortex interaction.

Nomenclature

$a1$ = longitudinal flapping angle of rotor tip path plane, positive when trailing edge of tip path plane is higher than leading edge
$b1$ = lateral flapping angle of rotor tip path plane, positive when retreating side of rotor tip path plane is higher than advancing side
c = chord of rotor blade
H = vertical distance between airframe axis and one-quarter chord line at rotor hub
R = rotor radius
r = radial location
U = flow velocity component parallel to tunnel axis, positive along tunnel freestream direction
U_∞ = tunnel freestream velocity
V = vertical component of velocity, positive downward
w = velocity component directed normal to rotor tip path plane, positive along rotor outflow direction (downward)
X = coordinate direction parallel to tunnel axis, origin at vertical line through center of rotor hub
Xb = distance along airframe axis measured from airframe nose
Xn = distance along airframe axis measured from vertical line through rotor hub pin
Y = lateral coordinate, origin at vertical plane through airframe axis
Z = vertical axis, origin at center of rotor hub
Δw = difference in measured values of w due to the airframe, found by subtracting the value with the airframe absent from that with the airframe present
θ = azimuthal location of measuring volume, measured from freestream direction
μ = advance ratio, ratio of tunnel freestream speed to rotor tip speed
Ψ = azimuthal location of quarter chord line of reference rotor blade, measured from freestream direction, = 0 along downstream radius of rotor tip path plane

Introduction

PREDICTION of the performance and dynamics of rotorcraft is made complex because of the strong flowfield interactions between components. Unlike fixed-wing aircraft, rotorcraft must operate with large sections of the vehicle immersed in the vortical flowfield generated by rotors, especially during the crucial phases of hover, ascent, low-speed flight, and landing. The wake of the main rotor involves strong vortices, flows over the airframe, and sometimes interacts with the tail rotor blades. The resulting interactions cause complex and often unexpected effects. Without a reliable method for predicting such flows at the design stage, the interaction effects are mostly undesirable. If such effects can be accurately modeled, however, designers can extract substantial benefits from interaction effects. For example, it is known that the rotor wake at high forward speed can cause strong lift forces on the airframe. Before such effects can be utilized, detailed knowledge of the flowfield is essential to make accurate predictions at the design stage. The objective of the present study is to gain a physical understanding of the interaction phenomena to aid analytical modeling and also to provide a data base on a simple configuration for validation of new codes.

Traditional methods for rotorcraft aerodynamic analysis use the fact that the flowfield is often dominated by strong vortices. The flowfield can be calculated to a good degree of accuracy using potential flow theory by considering the velocity field to be induced by these vortices. Validation and improvement of such methods, then, requires velocity field measurements. The flowfield is typically unsteady and three dimensional, with the vortices forming concentrated regions of high velocity gradients. To obtain unambiguous measurements in such flows, nonintrusive techniques are required; the best such technique available today is laser Doppler velocimetry.

The present study focuses on interactions between a rotor and a solid airframe model. The configuration used is generic. The phenomena observed will bear relevance to interactions between the main rotor and the fuselage of a rotorcraft,

Received Dec. 8, 1987; presented as Paper 88-0666 at the AIAA 26th Aerospace Sciences Meeting, Reno, NV, Jan. 11-14, 1988; revision received June 23, 1988. Copyright © 1988 by the American Institute of Aeronautics and Astronautics, Inc. All rights reserved.

*Graduate Research Assistant, School of Aerospace Engineering. Student Member AIAA.
†Assistant Professor, School of Aerospace Engineering. Member AIAA.
‡Professor, School of Aerospace Engineering. Member AIAA.

between a tail rotor and a tail boom, or between a main rotor and a tailboom. In any of these, the problem may be divided into two parts: the effects of the solid body on the flowfield and wake of the rotor, and the effects of the rotor wake on the flow around the body. Both of these are known to be strong effects in existing rotorcraft. In future designs, where the rotor disk loadings will be higher because of better engines now available and rotor-airframe spacing will be smaller for better agility, such interaction effects are expected to be more significant.

Present Scope and Objectives

Previous work on similar problems has been summarized in Ref. 1. The study of rotorcraft aerodynamic interactions is at a stage where rapid growth is occurring. The full-scale problem has too much geometric complexity and too many nonlinear flowfield phenomena to be accurately computed from first principles on existing computers. Therefore, methods are being developed using simplified formulations to tackle the dominant phenomena first, using configurations that are less costly to model than full-scale rotorcraft. Detailed data on simple configurations are required to support physical modeling. This is the rationale behind the present configuration and experimental effort.

In Ref. 1, measurements on this configuration were reported, emphasizing the velocity field in the immediate vicinity of the rotor and showing the effects of the airframe on this velocity field. The present paper reports on the other aspect of the interaction problem, namely, the effect of the rotor wake on the airframe. This paper aims to complete the definition of a test case on which extensive steady and time-resolved pressure measurements[2] and flow visualization results[3] have already been reported. As reported elsewhere,[4-6] this test case is being used to develop prediction methods for aerodynamic interactions.

The data reported here practically are devoid of compressibility effects, and the Reynolds numbers used here are very much smaller than those on full-scale rotorcraft. No attempt is made to simulate any particular existing or planned rotorcraft. The objective is to develop an unambiguous and well-understood case to serve as a first benchmark for interaction codes.

Facility Description

Figure 1 shows the test configuration installed in the John J. Harper Wind Tunnel. A cylindrical airframe model of 134-mm diameter with a hemispherical nose is sting-mounted below a two-bladed teetering rotor. The rotor shaft is powered by a 3-hp electric motor mounted above the test section. The rotor and the airframe are linked solely through the flowfield, and their relative positions can be varied. The rotor model is detailed in Fig. 2. The airframe is instrumented with 94 static pressure taps and 18 microphone ports. The rotor consists of two untwisted NACA 0015 blades of 86-mm chord rigidly attached to one another and mounted using a teetering pin assembly to the rotor shaft. The hub size is minimized by this design, at the expense of cyclic pitch control and flapping capability, to minimize contamination of the data by hub effects, which are difficult to model analytically. The stiffness of the blade eliminates coning. The blades are preset at 10-deg collective pitch. The rotor diameter is 0.914 m. The shaft is tilted forward 6 deg to simulate the forward flight condition. The rotor speed was held constant at 2100 rpm. The advance ratio μ, defined as the ratio of the tunnel freestream velocity to the rotor tip speed, was varied by varying tunnel freestream velocity.

Laser Velocimeter

The laser velocimeter used here is powered by a 5-W Argon laser and is operated in the backscatter mode. The data were collected in two stages, one for each component of velocity. This was made possible because the data could all be related to

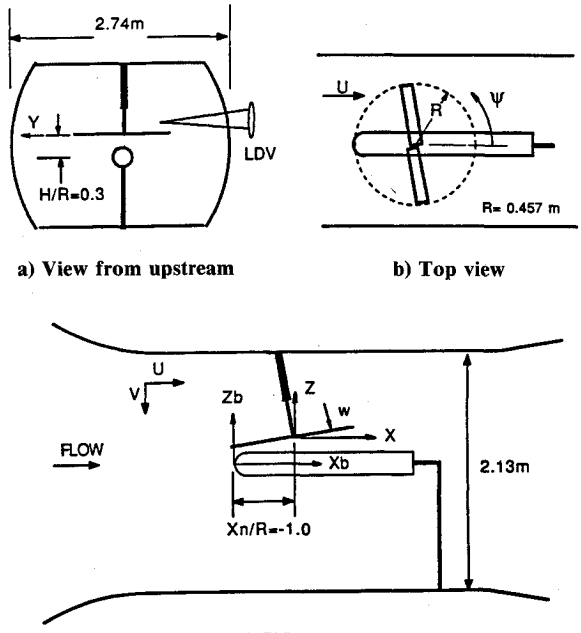

a) View from upstream b) Top view

c) Side view

Fig. 1 Rotor-airframe configuration.

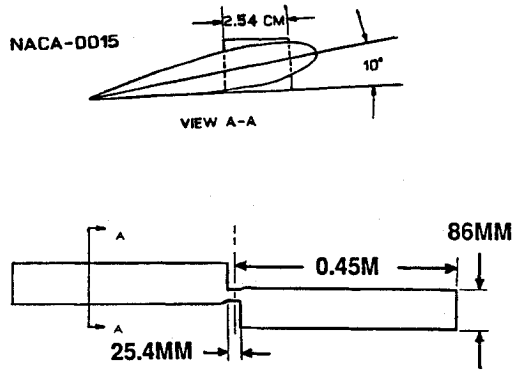

Fig. 2 Rotor blade details.

rotor azimuth, and no cross correlations between velocity components were sought. A frequency shifter was used to resolve flow direction and optimize accuracy of the data. The data were collected using a counter processor and transferred along with time-of-arrival information to an HP1000 computer.

Data Acquisition

The data acquisition and analysis scheme is shown in Fig. 3. At each measuring location, data were collected in blocks of 500 values, each data value being accompanied by a time-between-data (TBD) value. A once-per-revolution pulse from a rotor shaft encoder was used to sort the data according to the rotor azimuth when they arrived. When 60 such blocks had been sorted, giving a total of 30,000 data values, the results in each rotor azimuth interval were ensemble averaged to give the average velocity during that interval. The data shown in this paper were obtained with 6-deg azimuth resolution.

Experiments

Rotor Flowfield

An extensive set of measurements was performed in the close vicinity of the rotor tip path plane. These are discussed in detail in Ref. 1. For completeness, the overall features of

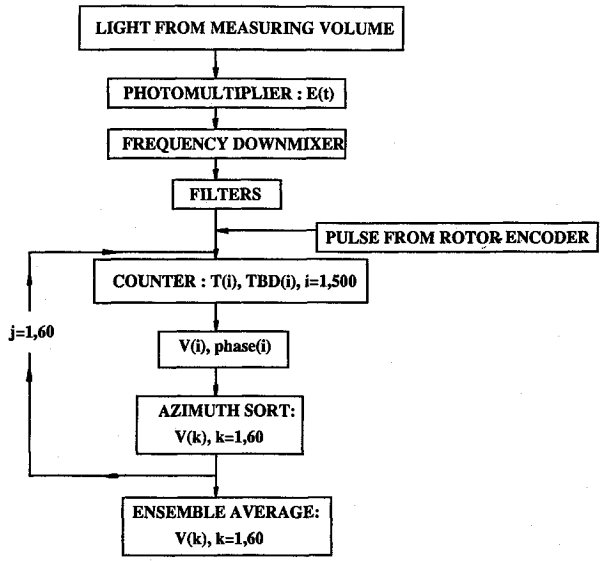

Fig. 3 Data acquisition scheme.

the flowfield immediately below the rotor are repeated in this paper. The tip path plane was determined using the laser beams and the LDV traverse system, by noting the positions where the beams were first touched by the bottom surface of the rotor blades, and applying simple geometry. This was repeated for every test condition, since the trajectory of the rotor blades depends on the balance between the aerodynamic and inertial forces and moments on the blades. Once the tip path trajectory was determined, a coordinate transformation was applied to determine a set of radial and azimuthal locations, each of which was located in a plane parallel to and 12.5 mm away from the bottom of this tip path disc. At each measuring location (a few locations were inaccessible to the LDV due to opaque obstacles), 30,000 data values were collected, as described before, and sorted according to the rotor orientation at their instants of arrival.

The features of the rotor wake flowfield can be seen in a time-averaged sense in Fig. 4. This contour plot was formed using the average of all 30,000 values of w, the component of velocity normal to the rotor disc, at each measuring location. The values are normalized using the freestream velocity and are positive downward. It is to be noted here that, in forming values of w, only the downward velocity V and the streamwise velocity U were used; the component along the optical axis of the LDV was not accessible. This definitely means that what is shown is not a complete picture of the normal component of velocity, and no claim can be made that the third component is small, in the absence of quantitative proof. The purpose of showing these data is to see the effect of the presence of the airframe on the measured velocity field. For purposes of comparison with computational results, the absence of the third component poses no fundamental difficulty; the computed results can very easily be resolved into components and compared one component at a time in detail.

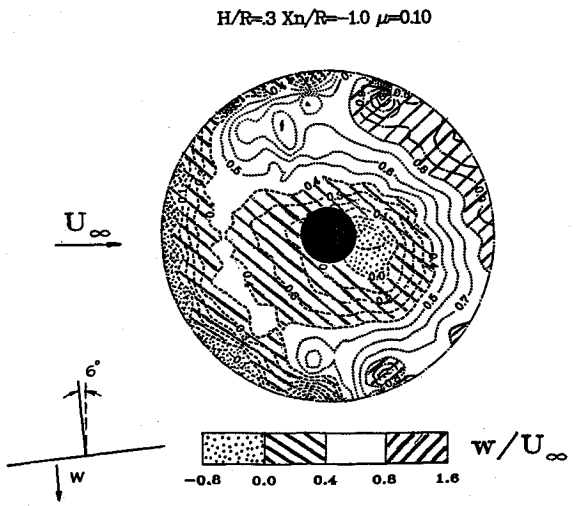

Fig. 4 Contour plot of the time-averaged downward velocity measured 12.5 mm below the rotor disc, negative values denote upflow.

The contour plot is seen to be asymmetric about the longitudinal axis. The strongest downflow occurs around 90 and 270 deg and in the region between 25 and 45 deg. Upflow exists near the tip region throughout the front part of the disk. There is also a region of upflow downstream of the hub where there is a pronounced interaction between the airframe and the flow downstream of the hub. This point will be further seen from the next figure. The flow downstream of the hub is complicated by several effects. First, the hub and rotor shaft induce flow separation. Second, the hub imparts a rotation, as well as periodic oscillations, to the flow near it. Third, this region starts at the center of the vortex system formed at the blade roots. These effects are not easy to include in prediction methods.

The interaction effect due to the presence of the airframe is shown in a time-averaged sense in Fig. 5. The data acquisition procedure used to obtain Fig. 4 was repeated, with and without the airframe present in the wind tunnel. The data set obtained without the airframe present was subtracted from that obtained with the airframe present. The resulting difference in w is plotted in Fig. 5. The magnitude of the difference in w is seen to be of the same order as w itself. The major effects are seen to be felt in a crescent over the front part of the airframe and along a strip downstream of the hub. These effects can be explained as follows. The upflow caused by the airframe is seen as a dip in the plot near the leading edge of the disc. The asymmetry between the two sides of the airframe can be attributed to the displacement of the wake and vortex trajectories by the airframe. The narrow region of increased upflow downstream of the hub is due to the close vicinity of the top of the airframe, which acts as an obstruction to the rotor wake.

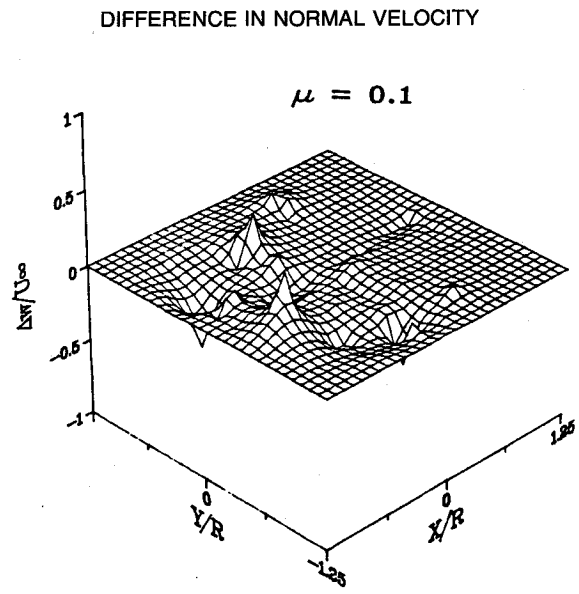

Fig. 5 Difference between the time-averaged velocity normal to the rotor disc, between measurements taken with and without the airframe present.

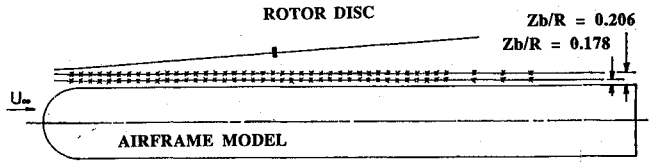

Fig. 6 Measurement locations.

Body Surface Measurements

Measurements along the body surface were performed at heights of 12.7 and 25.4 mm above the surface, as shown in Fig. 6. For each height, measurements were made at 43 points located directly above the static pressure ports on the body so that the results could be correlated with mean surface pressure measurements. As with the measurements close to the rotor tip path plane, these data were also acquired one component at a time. Since all data were referenced to the position of the rotor and phase averaged, this lack of simultaneity posed no problems, except that any nonperiodic fluctuations were averaged out. Previous investigations, reported in Ref. 3, have shown that these effects are negligible in this experiment. From the periodic velocity variation at each point, the tip vortex passage could be identified. The time of passage deduced from these data agreed well with the flow visualization results obtained by Brand et al.[3] Some measurements without the body present were performed at the same stations as in Fig. 6 to see the effect of the body surface flowfield on the tip vortex trajectory.

Results and Discussion

The instantaneous flowfield above the cylinder is illustrated schematically in Fig. 7. This picture was formed by extension of Gray's model for a hovering rotor[7] to the case of low-speed forward flight and confirmed by flow visualization.[3] The rotor induces an inflow above itself and causes a high-energy vortex-dominated wake to be blown down over the airframe. The dominant feature of this wake is the tip vortex. The trajectory of the vortex filament defines the edge of the wake and, in this case, is directed downward and streamwise. Immediately downstream of the tip vortex, the inboard vortex sheet may be observed. In flow visualization studies, this appears as a line of mild discontinuity in the flow pattern. From this picture, several features may be inferred. The induced velocity in the wake is directed upward just upstream of the tip vortex and is strongly downward just downstream of it. The nature of the bound circulation distribution on an untwisted rotor blade is shown in Fig. 8. The major difference with the distribution on a fixed wing is that the bound circulation peaks strongly at a point inboard of the tip. The radial derivative of the bound circulation changes sign at this location. The inboard vortex sheet thus has a sense of rotation that is opposite to that of the tip vortex. Because of this feature, the induced velocity inside the wake decreases strongly from that at the tip vortex.

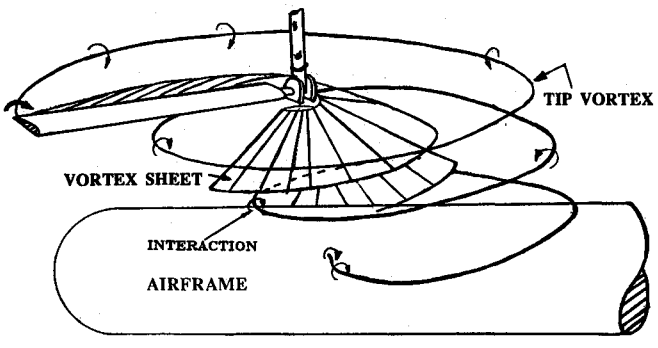

Fig. 7 Schematic representation of the instantaneous flowfield above the airframe, for a single-bladed rotor in low-speed forward flight.

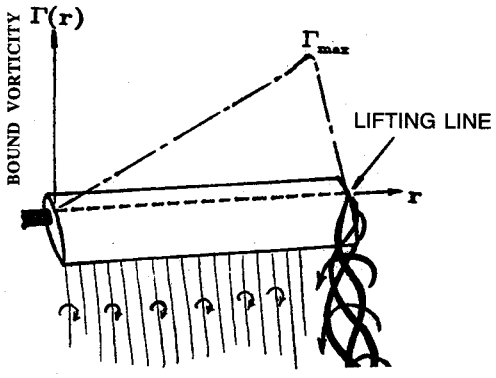

Fig. 8 Radial distribution of bound circulation on an untwisted rotor blade.

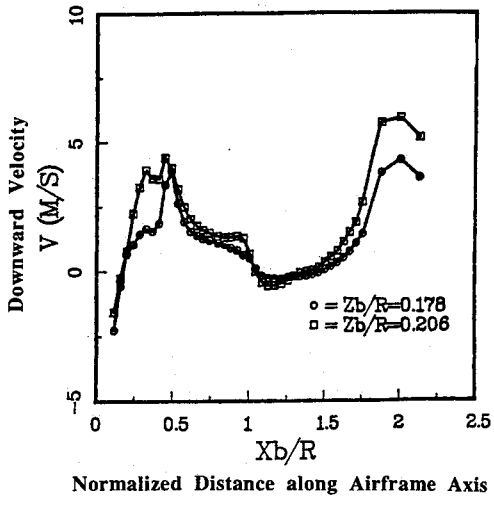

Fig. 9 Time-averaged downward velocity along lines parallel to the airframe axis above the airframe.

In Fig. 9, the time-averaged downward velocity V, measured along lines parallel to the cylinder axis and at two different heights above the cylinder, are shown. Several effects are visible. The cylinder nose causes upwash (negative values of V) just downstream of the nose. The hub, located at $Xb/R = 1$, produces an upwash downstream of it and accelerates and then decelerates the flow passing beneath it. The downward velocity decreases closer to the airframe because of the blockage caused by the cylinder. The peaks in the downward velocity at $Xb/R = 0.4$ and 1.8 correspond to the edges of the wake. Figure 10 shows the values of the streamwise velocity component U at the same stations. One unexpected effect is that the streamwise velocity U inside the wake increases near the airframe surface. This effect can be explained by considering the effect of the solid surface on the vortex sheet from the rotor. The sense of rotation in the vortex sheet is such that the surface induces an additional velocity in the streamwise direction. For the constant-chord untwisted rotor blades used, the vortex sheet has a sense of rotation opposite to that of the tip vortices.

Figure 11 shows the effect of the airframe on the flowfield close to the airframe nose. This is gauged by looking at the time-averaged downward velocity, measured at several stations along a line 12.5 mm above the top of the airframe, with and without the airframe present. The data shown are only those over the forward portion of the airframe, starting from the nose and ending under the rotor hub. The peak in the downward velocity, corresponding to the leading edge of the wake, occurs at about $Xb/R = 0.55$ when the airframe is not present. When the airframe is present, this peak is moved

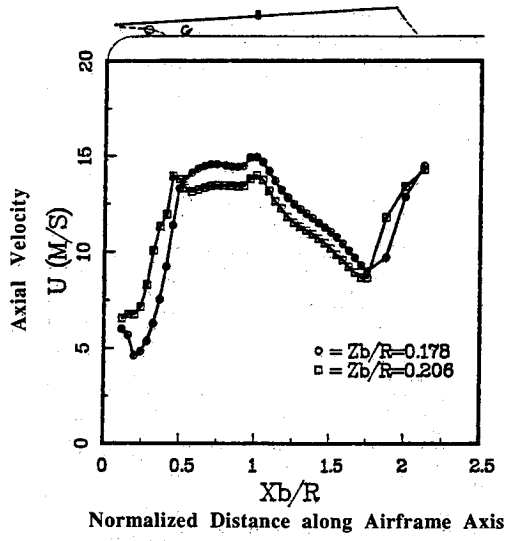

Fig. 10 Time-averaged axial velocity along lines parallel to the airframe axis above the airframe.

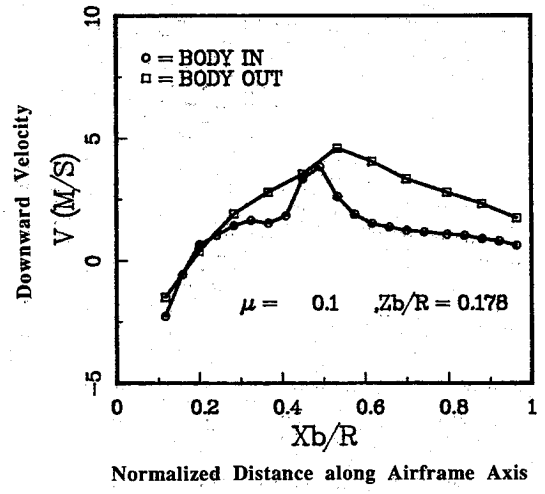

Fig. 11 Effect of the presence of the airframe on the downward velocity component close to the airframe nose.

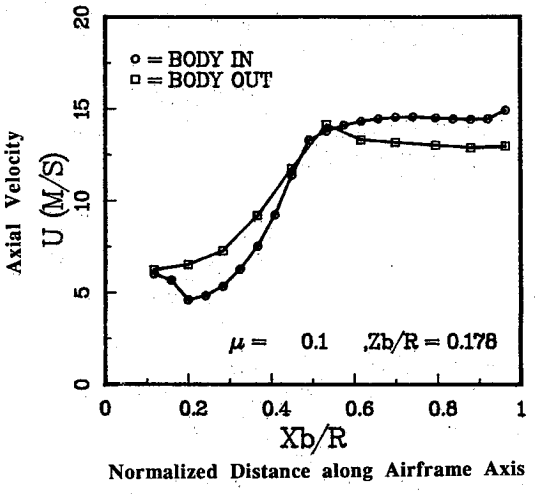

Fig. 12 Effect of the presence of the airframe on the axial velocity component close to the airframe nose.

upstream to $Xb/R = 0.5$. This can be explained by considering the image effect of the surface on the tip vortex; indeed, this was clearly confirmed by flow visualization. The downward velocity is decreased slightly when the airframe is present, due to the blockage effect of the airframe. Figure 12 shows that the streamwise velocity for the same case is lower outside the wake and higher inside with the body present. This is because when the airframe is absent, the wake leading edge is further downstream and, hence, the blockage effect is less. Inside the wake, the body surface acts as a mirror plane for the trailing vortex sheet and accelerates the flow. Thus, it is seen that one effect of the presence of the cylinder is that the tip vortex and the vortex sheet are forced apart. This, in turn, may be expected to change the relative times at which the effects of these features are felt at the surface of the cylinder.

Figure 13 shows the variations in downward velocity over the front portion of the airframe in greater detail. Here, the azimuthal variation of the downward velocity at each measuring point is plotted. Again, the measuring points are all along a horizontal line, located at $Zb/R = 0.178$. The data shown cover the distance from the airframe nose to $Xb/R = 0.7$, where the effects of vortex interaction at the edge of the wake are felt strongly. Looking at the azimuthal variation in downward velocity at about $Xb/R = 0.6$, one sees several peaks appearing. The data do not repeat exactly from one blade to the next in this case. This is partly due to resolution problems in the plot and partly due to the fact that blade-to-blade repeatability was not precise during vortex-surface interactions. Figure 14 shows data at the same locations with the airframe removed. It is clear that without the interference of the airframe there is only one sharp, high peak for each vortex passage across the measuring location. However, as shown in Fig. 13, the presence of the airframe causes two or three peaks to appear at the vortex impingement locations, indicating breakup of the vortex structure. The strength of the tip vor-

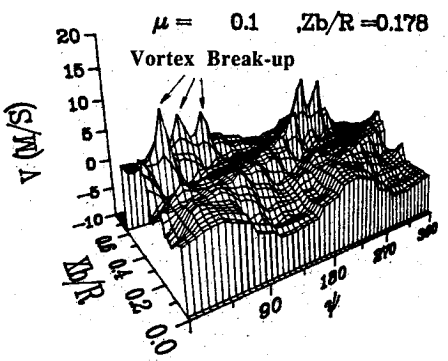

Fig. 13 Azimuthal variation of downward velocity along a line 12.7 mm above the top of the airframe.

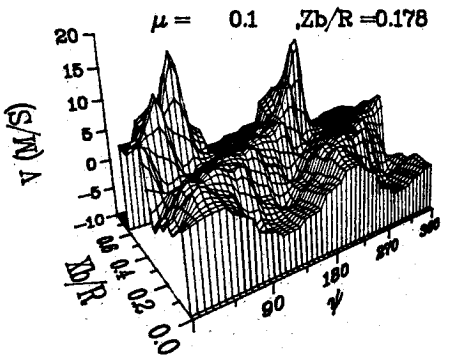

Fig. 14 Azimuthal variation of downward velocity at the same spatial locations as in Fig. 13, with the airframe removed.

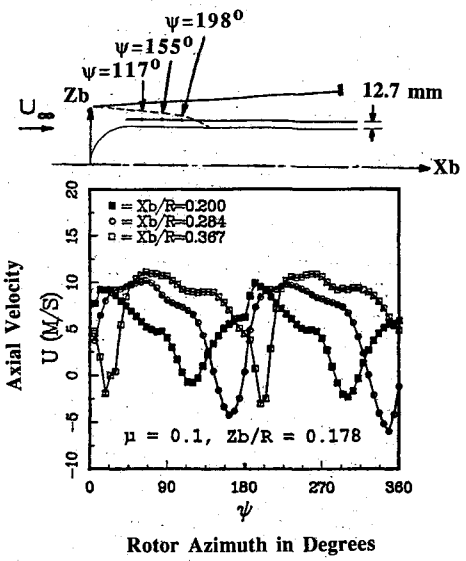

Fig. 15 Azimuth-resolved axial velocity at 3 points above the airframe, showing the effects of a close vortex passage.

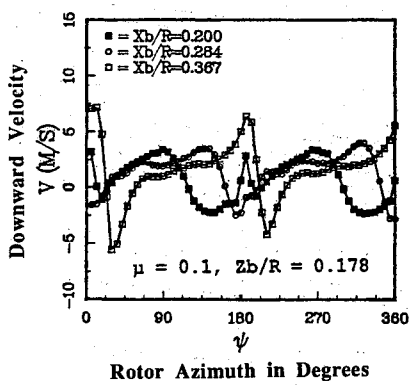

Fig. 16 Azimuth-resolved downward velocity at the points shown in Fig. 15.

tices is also reduced when the airframe is present. The multiple peaks in Fig. 13 can only be attributed to the breakup of the strong tip vortex, with the creation of secondary vortical structures. The precise structure and nature of these secondary features remains to be investigated. For instance, it is unclear what effect the boundary layer at the surface has on the origin of these features. One strange result is that the multiple-peak feature has not been observed in the time-resolved surface pressure distributions to date.

Figures 15 and 16 show the azimuth-resolved velocity at three points just above the airframe surface. The sharp dips in axial velocity shown in Fig. 15 correspond to the passage of the tip vortex, as confirmed by flow visualization. The trajectory of the vortex is shown schematically above Fig. 15. The velocity measured at $Xb/R = 0.200$ shows the effect of the velocity induced by the vortex as it passes above. The axial velocity changes from a value essentially close to the freestream to approximately stagnating conditions at about 117 deg when the vortex is directly above. At this instant, the vertical velocity is crossing zero, as would be expected. The effects are sharper at $Xb/R = 0.284$, where the axial velocity shows substantial reversed flow at about 150 deg, as the vortex passes much closer to the measuring point. Again, at this instant, the vertical velocity is changing from being downward (downstream of the vortex) to being upward (after the vortex center passes). As the vortex approaches the measuring point, the peak becomes narrower and sharper. The data at $Xb/R = 0.367$ show very rapid changes. The vertical velocity shown in Fig. 16 exhibits the typical vortex velocity profile as the core passes very close to the measuring point. The convection of the vortex is also apparent in these figures from the phase shift of these features.

Concluding Remarks

The rotor wake causes large periodic and time-averaged effects on the airframe flowfield. It is altered by the presence of the airframe, but these changes can generally be interpreted and, therefore, perhaps be calculated using simple vortex theory if details of the vortex strengths and structure are known.

The dominant feature of this flowfield is the presence of strong tip vortices. Interactions of these vortices with the cylinder, as well as the dynamics of these vortices, cause strong effects in the flowfield. The presence of the cylinder clearly causes significant changes in these vortex structures and appears to cause breakup into several different structures.

The velocity field close to the cylinder shows that the tip vortex structure is decelerated and the inboard vortex sheet is accelerated by the presence of the cylinder. This is qualitatively consistent with expectations based on two-dimensional concepts such as image planes for these vortices. Vortex interaction is also seen to cause transient flow stagnation and reversal immediately above the surface.

Acknowledgments

This work was sponsored by the U.S. Army Research Office under Contract DAAG29—82-K0084, the Center of Excellence in Rotary Wing Aircraft Technology program. Robert E. Singleton and Thomas Doligalski were the Technical Monitors. The authors gratefully acknowledge the assistance of Albert Brand, who amassed the flow visualization data used to interpret many features of the velocity field.

References

[1]Liou, S. G., Komerath, N. M., and McMahon, H. M., "Velocity Measurements of Airframe Effects on a Lifting Rotor in Low-Speed Forward Flight," *Journal of Aircraft*, Vol. 26, No. 4, April 1989, pp. 340–348.

[2]Brand, A. G., McMahon, H. M., and Komerath, N. M., "Surface Pressure Measurements on a Rotor-Airframe Configuration in Forward Flight," *AIAA Journal*, Vol. 27, No. 5, May 1989, pp. 569–574.

[3]Brand, A. G., Komerath, N. M., and McMahon, H. M., "Results from Laser Sheet Visualization of an Incompressible Vortex Wake," AIAA Paper 88-0192, Jan. 1988.

[4]Egolf, T. A., and Lorber, P. F., "An Unsteady Rotor/Fuselage Interaction Method," *Proceedings of the American Helicopter Society Specialists' Meeting on Aerodynamics and Aeroacoustics*, Arlington, TX, 1987.

[5]Berry, J. D., "Prediction of Time-Dependent Fuselage Pressures in the Wake of a Helicopter Rotor," *Proceedings of the 2nd International Conference on Rotorcraft Basic Research*, U.S. Army Research Office, 1988.

[6]Mavris, D. M., Komerath, N. M., and McMahon, H. M., "Prediction of Unsteady Rotor-Airframe Aerodynamic Interactions," AIAA Paper 88-4420, Sept. 1988.

[7]Gray, R. B., "An Aerodynamic Analysis of a Single-Bladed Rotor in Hovering and Low-Speed Forward Flight as Determined From Smoke Studies of the Vorticity Distribution in the Wake," Princeton Univ., Aeronautical Engineering Dept., Princeton, NJ, Rept. 356, Sept. 1956, p. 65.